Development 121, 3131-3140 (1995)
Printed in Great Britain © The Company of Biologists Limited 1995

The dorsal involuting marginal zone stiffens anisotropically during its convergent extension in the gastrula of *Xenopus laevis*

Steven W. Moore[1,2,*], Raymond E. Keller[2] and M. A. R. Koehl[1]

[1]Department of Integrative Biology, University of California, Berkeley, CA 94720-3140, USA
[2]Department of Molecular and Cell Biology, University of California, Berkeley, CA 94720-3200, USA

*Author for correspondence at current address: Earth Systems Science, CSU Monterey Bay, 100 Campus Center, Seaside CA 93955-8001, USA

SUMMARY

Physically, the course of morphogenesis is determined by the distribution and timing of force production in the embryo and by the mechanical properties of the tissues on which these forces act. We have miniaturized a standard materials-testing procedure (the stress-relaxation test) to measure the viscoelastic properties of the dorsal involuting marginal zone, prechordal mesoderm, and vegetal endoderm of *Xenopus laevis* embryos during gastrulation. We focused on the involuting marginal zone, because it undergoes convergent extension (an important and widespread morphogenetic process) and drives involution, blastopore closure and elongation of the embryonic axis. We show that the involuting marginal zone stiffens during gastrulation, stiffening is a special property of this region rather than a general property of the whole embryo, stiffening is greater along the anteroposterior axis than the mediolateral axis and changes in the cytoskeleton or extracellular matrix are necessary for stiffening, although changes in cell-cell adhesions or cell-matrix adhesions are not ruled out. These findings provide a baseline of data on which future experiments can be designed and make specific, testable predictions about the roles of the cytoskeleton, extracellular matrix and intercellular adhesion in convergent extension, as well as predictions about the morphogenetic role of convergent extension in early development.

Key words: biomechanics, gastrulation, *Xenopus*, convergent extension, mesoderm

INTRODUCTION

The tissues of an embryo change shape and move relative to each other during morphogenesis. Physically, deformations of any object are caused by mechanical forces acting on and within it. The nature and extent of these deformations depend on the geometry and mechanical properties (e.g., stiffness) of the object. Thus, all processes that affect morphogenetic tissue movements and deformations must do so by influencing, either directly or indirectly, the distribution, magnitude, or timing of forces or mechanical properties within the embryo.

To understand morphogenesis, we must work out the connections between molecular events and the mechanical events occurring at higher levels of organization (cell, tissue, embryo). An important step toward that goal is the development of experimental systems in which the biomechanics of morphogenetic processes can be quantified during experiments that manipulate the expression of particular genes or the function of their products. In this paper, we measure normal changes in the mechanical properties of the involuting marginal zone (IMZ), prechordal mesoderm and vegetal endoderm of *Xenopus laevis* embryos during gastrulation (Fig. 1A). We focus primarily on the IMZ, because it plays an important biomechanical role in gastrulation, and because it serves as an excellent system for studying the molecular and cellular basis of a fundamental morphogenetic process: *convergent extension.*

Convergent extension

During convergent extension, a tissue narrows along one axis while extending along a perpendicular axis (Keller, 1986). Examples of the morphogenetic roles of convergent extension have been documented for insects (Irvine and Wieschaus, 1994), echinoderms (Ettensohn, 1985; Hardin and Cheng, 1986), and various chordates such as ascidians (Miyamoto and Crowther, 1985), fish (Warga and Kimmel, 1990; Trinkaus et al., 1992), amphibians (Vogt, 1929; Jacobson, 1981; Keller and Danilchik, 1988) and birds (Schoenwolf and Alvarez, 1989). Convergent extension usually involves cell intercalation, the rearrangement of cells to form a longer, narrower tissue, although other events, including change in cell shape and oriented cell divisions (Schoenwolf and Smith, 1990; Condic et al., 1991), may also contribute.

In *X. laevis* embryos convergent extension of both the dorsal IMZ and the dorsal non-involuting marginal zone (NIMZ) plays a critical role in gastrulation (reviewed in Keller, 1986). During gastrulation the dorsal IMZ, including the Spemann organizer (Spemann, 1938), involutes into the interior of the

embryo where its deep mesenchymal cells form the notochordal and somitic mesoderm and its superficial epithelial cells form the endodermal roof of the archenteron; the dorsal NIMZ remains on the outside of the embryo and forms the posterior neural plate (Keller, 1975; 1976) (Fig. 1A). Cultured explants of both the dorsal IMZ and the dorsal NIMZ autonomously converge and extend, demonstrating that these movements are active, intrinsic to these regions and independent of forces generated elsewhere in the embryo (Keller and Danilchik, 1988).

Convergent extension of the IMZ is more forceful than that of the NIMZ. Sandwiches of two dorsal marginal zones (Keller and Danilchik, 1988) can push anteroposteriorly with a force of 1.2 μN (Moore 1992; 1994), corresponding to at least 0.6 μN per dorsal axis. During these measurements, the combined length (IMZ + NIMZ) was fixed and IMZ extension overpowered NIMZ extension, compressing the NIMZ (Moore, unpublished observations).

Moreover, convergent extension of the IMZ plays a major role in *X. laevis* gastrulation. Convergence of the IMZ occurs in the mediolateral direction, around the circumference of the blastopore, causing its involution and squeezing the blastopore shut (Keller, 1986; Keller et al., 1992; Keller and Jansa, 1992). Extension occurs in the anteroposterior direction, thus elongating the body axis (Jacobson, 1981; Keller et al., 1991; 1992) (Fig. 1A). When these movements do not occur in embryos ventralized by UV irradiation, gastrulation is abnormal and the embryo remains spherical (Scharf and Gerhart, 1980).

Stiffness of the IMZ

There are several compelling and interrelated reasons to analyze changes in the stiffness (resistance to deformation) of the IMZ during convergent extension:

(1) During convergent extension, the IMZ becomes both longer and narrower. Beam theory tells us that the maximum force a column can support without buckling (collapsing by bending), is proportional to the column radius raised to the fourth power and inversely proportional to the column length squared (Wainwright et al., 1976). Thus, in an elongating column of constant volume, halving the radius quadruples the length and reduces the force that can be supported by 64-fold! Buckling force is also proportional to the stiffness of the column material, so the IMZ could compensate for its increasingly slender geometry by increasing its stiffness, thereby allowing it to extend and distort neighboring, passive tissues without buckling under the load.

(2) Increased stiffness must be developmentally regulated to occur only after the IMZ bends sharply around the blastopore lip during involution. Grafts of postinvolution IMZ from a mid-gastrula embryo to the outer preinvolution region of an earlier embryo do not involute when they reach the blastoporal lip but sit on the lip like a canoe at the edge of a waterfall (Keller, 1986), as if too stiff to turn the corner.

(3) The cell motility underlying convergent extension of the IMZ is known (see Shih and Keller, 1992a). Convergent extension occurs as the deep mesodermal cells form protrusions directed medially and laterally in the embryo. This bipolar activity apparently exerts anisotropic traction on adjacent cells, pulling them together and narrowing the tissue mediolaterally, while extending the tissue anteroposteriorly (Fig. 2). Thus, this region is an ideal experimental system in which to explore how cell motility, cell adhesion and the molecules involved in these processes function in the mechanical processes of convergent extension and gastrulation.

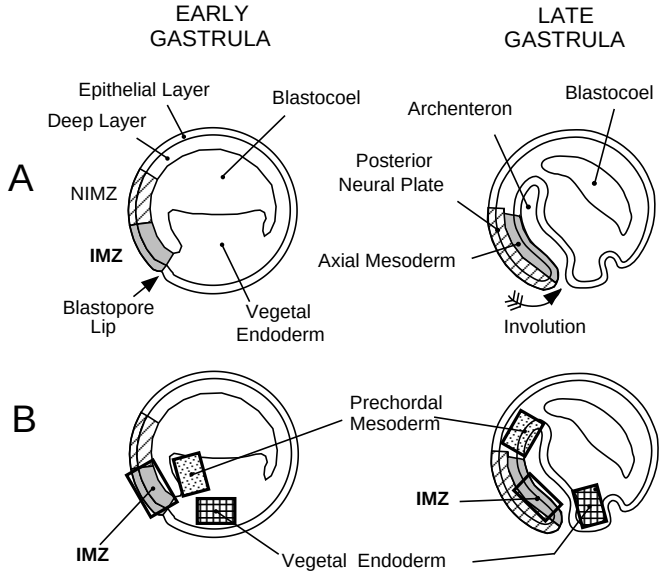

Fig. 1. (A) Diagrammatic saggital sections through early and late *X. laevis* gastrulae. Dorsal is to the left and anterior is upward. (B) Location on embryo from which IMZ, prechordal mesodermal and vegetal endodermal explants were taken.

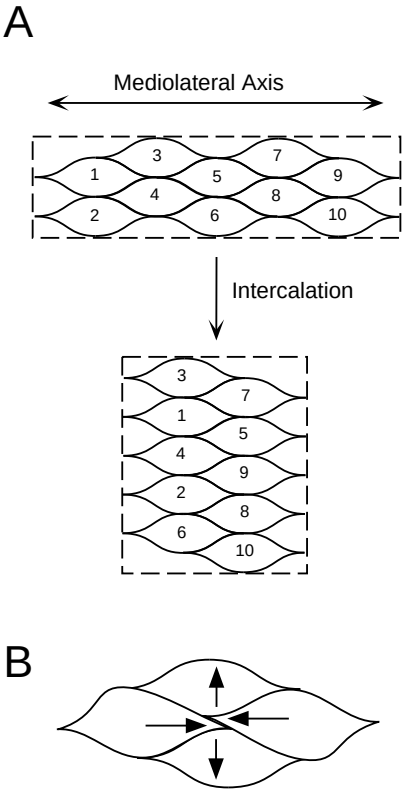

Fig. 2. (A) Anteroposterior extension of a tissue by mediolateral cell intercalation. (B) Probable mechanism of convergent extension in the IMZ: cells crawl mediolaterally, wedging between neighbors and forcing them apart along the anteroposterior axis.

Specifically, for cell intercalation to push and form a stiff tissue column able to bear a load, the cells must be tightly adherent at their medial and lateral ends and reinforced against excessive mediolateral elongation. This anisotropic behavior could involve changes in the cytoskeleton, changes in the extracellular matrix, changes in cell-cell or cell-matrix adhesions, or changes in any combination of the four. It is essential to establish baseline measurements of morphogenetically important mechanical properties of the IMZ and to know how these change during gastrulation so that the specific mechanical roles of various cytoskeletal, matrix and adhesion molecules can be tested experimentally.

Objectives of this study

We used standardized engineering methods (described below) to quantify mechanical properties of *X. laevis* gastrula tissues. We focused on the dorsal IMZ, which undergoes convergent extension, and compared it with the prechordal mesoderm, which undergoes the contrasting morphogenetic movement of directed migration (Winklebauer et al., 1991), and with the vegetal endoderm, which is passively squeezed into the interior of the embryo during gastrulation (Keller and Winklebauer, 1992). Using this information, we have developed simple network models that quantitatively describe essential features of the viscoelastic behavior of these tissues, and we have answered the following questions important in our understanding of how these tissues function in morphogenesis:

(*1) Does the IMZ stiffen during development?* To answer this question, we compared the stiffness of explants of the IMZ prior to its involution and after its involution.

(*2) Is IMZ stiffness anisotropic?* We answered this question by measuring the stiffness of IMZ explants compressed either anteroposteriorly or mediolaterally, both before and after IMZ involution.

(*3) Does the mechanical response of the IMZ to an imposed strain depend on cell-shape changes or on cell rearrangement?* Measurements of cell shapes and positions during stress-relaxation tests answered this question and enabled us to make predictions about the role of intracellular versus intercellular or extracellular components in the changes in mechanical properties observed.

(4) If the IMZ becomes stiffer, is this change a general property of all gastrula tissues, or is it specifically related to convergent extension of the IMZ? To answer this question, we compared the change in anteroposterior stiffness of the converging and extending IMZ with that of the prechordal mesoderm and vegetal endoderm.

A biomechanical approach

To perform a rigorous mechanical analysis of convergent extension, we must replace qualitative observations, such as those above, with standardized engineering measurements of the mechanical properties of embryonic tissues (e.g., Koehl et al., 1990; Moore, 1994). Mechanical engineering techniques have been used to study biological processes at the organismal and tissue levels (e.g. Wainwright et al., 1976; Fung, 1977; Vogel, 1988; 1994; Vincent 1990), the cellular level (reviewed in Akkas, 1987; 1990; Bereiter-Hahn et al., 1987; Bray, 1992) and the subcellular level (Finer et al., 1994; Ishijima et al., 1991; Svoboda and Block, 1994), but application of biomechanics to the study of morphogenesis is still in its infancy (see Mittenthal and Jacobson, 1990; Koehl, 1990).

One difficulty associated with quantifying the stiffness of embryonic tissues is that they, like other biological materials (see Bereiter-Hahn et al., 1987; Fung, 1977), are *viscoelastic* – that is, the force required to deform them depends not only on how far they are deformed (like an elastic solid), but also on how fast and for how long (like a viscous fluid) (see Koehl, 1990; Moore, 1994). In this study, we quantify the viscoelastic properties of the IMZ by using a *uniaxial compressive stress-relaxation test*. This test yields a standardized stiffness measure that is largely independent of the measurement technique used. Therefore, our measurements, unlike those from most earlier studies (reviewed in Moore, 1992), can be compared directly with related data from other sources and used in mathematical models of morphogenesis (see Koehl, 1990).

Stress-relaxation tests

Stress-relaxation tests quantify the time-dependent mechanical behavior of viscoelastic materials in a manner that is independent of the physical dimensions of the sample used for the test (e.g. Ferry, 1970; Findley et al., 1976; Fung, 1977). During a uniaxial compressive stress-relaxation test, a sample block of material (e.g. tissue) of initial length L_o is compressed rapidly between two parallel surfaces to a shorter length (L) at which it is held (Fig. 3) while the force (F) required to maintain length L is monitored for a period of time. The sample's deformation is expressed as strain ($\varepsilon=(L-L_o)/L_o$), which is negative for compression, and mechanical force is expressed as *stress* ($\sigma=F/A$, where A is the cross-sectional area of material bearing the force), which, by convention, is also negative for compression. Using stress and strain factors out the dimensions of the sample, so results from differently sized pieces of material can be compared. In viscoelastic materials the stress required to

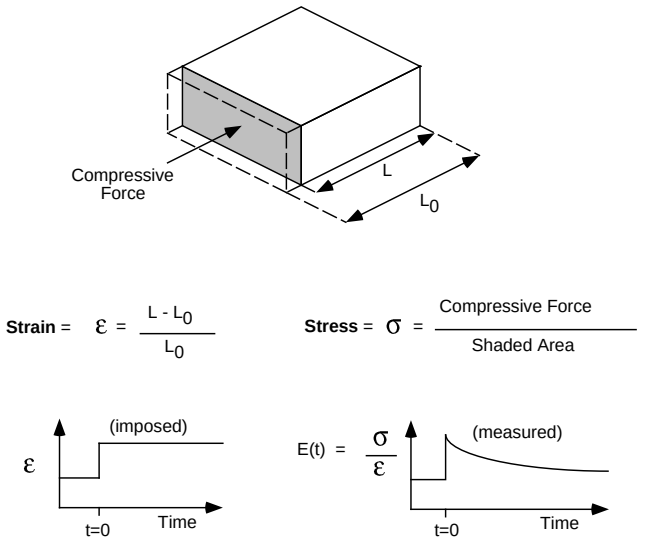

Fig. 3. Stress-relaxation test in uniaxial compression. A finite strain is imposed on a block of material and then held constant. The stress required to maintain the strain is recorded as a function of time and the relaxation function of the material is obtained by plotting the stress per unit strain as a function of time.

maintain constant strain decreases with time. The stiffness of such materials can be expressed as a *time-dependent elastic modulus* ($E(t)=\sigma(t)/\varepsilon$, where ε is the strain applied to the material and $\sigma(t)$ is the stress in the material t seconds after the strain is applied). Since both σ and ε are negative for compression, E is positive. (Some texts, such as Fung 1977, use the symbol '$k(t)$' rather than '$E(t)$' for time-dependent modulus.) Plotting $E(t)$ against time yields a curve called the *relaxation function* of the material. A measured relaxation function may consist of thousands of data points. To facilitate comparisons between different relaxation functions, it is conventional either to focus on the value of the curves at a few specific points in time, which is what we do for the statistical comparisons discussed in this paper, or to approximate the curves with simple mathematical expressions.

Mechanical network models

Mathematical expressions used to approximate empirical relaxation functions may themselves be expressed as *mechanical network models*. These models represent viscoelastic materials as a collection of *springs* (elastic elements, each with a particular stiffness) and *dashpots* (fluid elements, each with a particular viscosity) (Fig. 7) (see Koehl, 1990; Findley et al., 1976). Spring-dashpot models contain exactly the same information as the corresponding equations, but they present it differently, explicitly separating the relative contributions of elastic (solid-like) and viscous (fluid-like) properties to the overall mechanical properties of the material. Network model descriptions of mechanical properties of embryonic tissues are used in mathematical models of morphogenetic processes (e.g. Davidson et al., 1995; Odell et al., 1981; Weliky and Oster 1990; Weliky et al. 1991); therefore, empirical determinations of the mechanical properties of embryonic tissues should yield elasticity and viscosity values for the springs and dashpots of a network model if they are to be useful in quantitative models of morphogenesis. We provide such values here.

MATERIALS AND METHODS

Embryo and explant preparation

Eggs were fertilized and dejellied by standard methods (see Kay and Peng, 1991) and held at 17°C in one-third strength Modified Barth's Solution (MBS). Shortly before use, embryos were transferred to modified Danilchik's solution (DFA; Sater et al., 1993) plus bovine serum albumen (BSA, 1 g/l) and allowed to warm to room temperature (approx. 22°C). DFA mimics amphibian blastocoel fluid in composition and supports normal deep cell behavior (see Shih and Keller, 1992a). BSA coats glass and plastic, thus reducing adhesion and friction (see Keller, 1991). Embryos were staged according to Nieuwkoop and Faber (1967). Explants (Fig. 1B) were made from early (stage 10+; before most IMZ involution) or late (stage 11.5; after most IMZ involution) gastrulae, using eyebrow hair knives (see Keller, 1991) to remove square pieces of tissue roughly 400 μm on a side.

Measurement of time-dependent elastic modulus

The time-dependent elastic modulus, E(t), of each explant was measured by conducting a uniaxial compressive stress-relaxation test using the 'Histowiggler' (Fig. 4), a mechanical testing apparatus designed by Moore (1992, 1994). Immediately after excision, the explant was placed for either anteroposterior or mediolateral compression on a small stage of glass coverslip fragments (Fig. 5) mounted on an aluminum arm and positioned in the DFA-filled test chamber of the Histowiggler. A three-minute stress-relaxation test with 0.2 strain (i.e., the explant was compressed to 80% of its original length) was initiated as soon as possible, generally within 5 minutes of explantation. Experiments were done at room temperature (approximately 22°C). If control embryos did not develop normally, data from that batch of embryos were discarded.

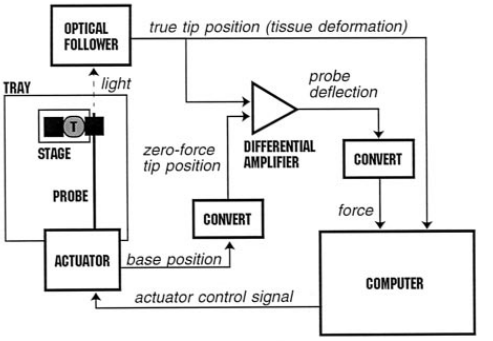

Fig. 4. (A). Schematic diagram of the 'Histowiggler' mechanical testing apparatus. Explanted tissue 'T' rests on a stage submerged in a small tray of DFA solution. Moving the stage toward the probe compresses the explant between a backstop glued to the stage and a square coverslip fragment glued to the flexible optical fiber probe (see Fig. 5). A computer monitors probe tip position (by following light transmitted through the probe) and also controls tip movements (indirectly, through actuators attached to the probe base). Base position information is used to estimate where the probe tip would be if no force were bending the probe. By subtracting this 'zero-force tip position' from the actual tip position and then multiplying by probe stiffness, the computer calculates the force on the explant. During stress-relaxation tests, the computer was programmed to move the probe base as required to prevent tip displacement, so strain was controlled entirely by stage movement. Position resolution of the Histowiggler is 0.1 μm; force resolution is 0.02 μN.

Before and during each stress-relaxation test, the explant was videotaped from above (Fig. 5) and from the side through a dissecting microscope. The length (before and after compression), width and thickness of each explant were measured to the nearest 10 μm from these video records using NIH Image software on an Apple Quadra computer equipped with a Scion LG-3 image board. Although the explants were cut as rectangles, they rounded somewhat during the five-minutes when they were being mounted. It was initially unclear whether lateral bulges on a rounded explant contributed to resisting the compressive force, so we measured tissue width and thickness in two ways. The first method used the maximum width (white arrow in Fig. 5) and thickness of each specimen; this assumes the maximum cross-section of the specimen resists the compression and underestimates $E(t)$ if that assumption is invalid. The second method used the average width (black arrow in Fig. 5) and thickness of the contact areas of the specimen with the Histowiggler backstop and probe; this assumes the bulges do not contribute to resisting the force and overestimates $E(t)$ if that assumption is invalid. To determine which assumption was more suitable, E(50)s calculated each way were plotted as a function of the 'bulge index' (BI = the width obtained when bulges are included divided by the width when bulges are not included), a measure of the degree of rounding-up of the explant (Fig. 6). The first method appears least affected by variations in bulge size, suggesting that bulges do contribute significantly to resisting compression. Consequently, we have included bulges when calculating the $E(t)$s discussed in the remainder of this paper.

Measurement of cell shapes and positions during stress-relaxation

Explants were prepared as described above, and placed, deep cells

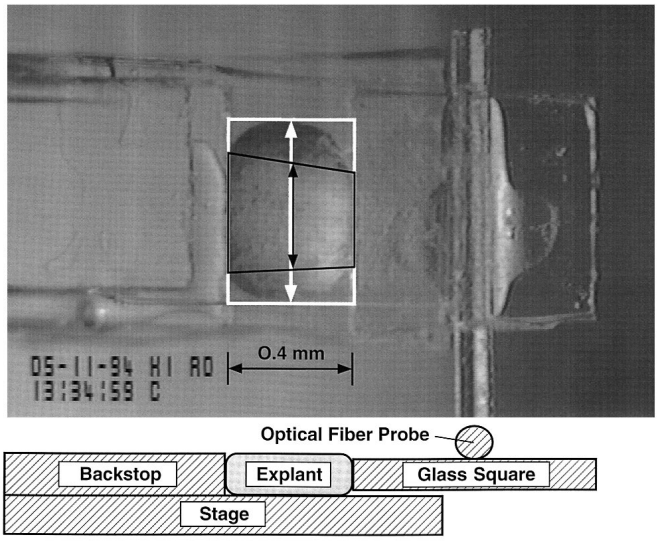

Fig. 5. Video image and end-view diagram of IMZ explant on Histowiggler stage showing relative positions of explant, probe with attached square of glass and stage with attached backstop. The two-headed arrows indicate the width of this explant measured when bulges on the tissue were included (white arrow) or ignored (black arrow).

down, in a Petri dish with a glass coverslip floor. The deep mesodermal cells were videotaped through a Nikon Diaphot inverted microscope using epi-illumination while we used the flat edge of a coverslip fragment mounted on a micromanipulator to compress the explant against an immobile backstop, mimicking the compressive strain of Histowiggler stress-relaxation tests. The video record was made for 5-10 minutes at approximately 650×, so cell boundaries could be seen and measured easily. Cell lengths (parallel to the axis of strain), widths (perpendicular to the axis of strain) and positions were measured to the nearest 2 μm using the Quadra system described above. Approximately 20 cells, whose boundaries were clearly visible throughout the video record, were measured on each explant.

Statistical analyses

To compare stiffnesses we used $E(180)$. This time choice represents a compromise; longer times might be more appropriate to the slow deformations occurring in embryos but also are subject to artifacts of healing. Mann-Whitney-U tests (performed with Statview Software, version 4.02) were used to make the statistical comparisons, and differences were assumed to be significant if $P<0.05$.

Network models

To provide mechanical data suitable for use in mathematical models of morphogenetic processes, we quantitatively described the elastic (solid-like) and viscous (fluid-like) properties of each explant using a lumped linear mechanical network model. Based on the general form of the measured relaxation functions, we chose a model (Fig. 7) composed of a spring in parallel with a Maxwell element (a spring and dashpot in series). The methods used to determine E_P (the elastic modulus of the parallel spring) and E_S and η (the elastic modulus of the spring and the viscosity of the dashpot, respectively, in the Maxwell element) are described in the Appendix.

RESULTS

Time-dependent modulus

The relaxation functions of IMZ, prechordal mesodermal and vegetal endodermal tissues were typical of viscoelastic materials; they began with a sharp peak (at the moment of strain application) but then declined, rapidly at first, and then more slowly, nearly leveling off by 180 seconds after strain application (Fig. 8). For example, the IMZ at stage 10+, when compressed anteroposteriorly (i.e., along its normal axis of extension) had a mean 'instantaneous' modulus, $E(0)$, of 21.3 N/m^2 (s.d.=5.7, n=15), which fell to an $E(180)$ of 3.9 N/m^2 (s.d.=1.5, n=15). Similarly, the IMZ at stage 11.5 had a mean anteroposterior $E(0)$ of 43.8 N/m^2 (s.d.=20.5, n=19), which fell to an $E(180)$ of 14.2 N/m^2 (s.d.=7.6, n=19). These moduli are 4 or 5 orders of magnitude lower than biological rubbers such as resilin or elastin (see Wainwright et al., 1976). $E(180)$ data for all three tissue types are summarized in Table 1.

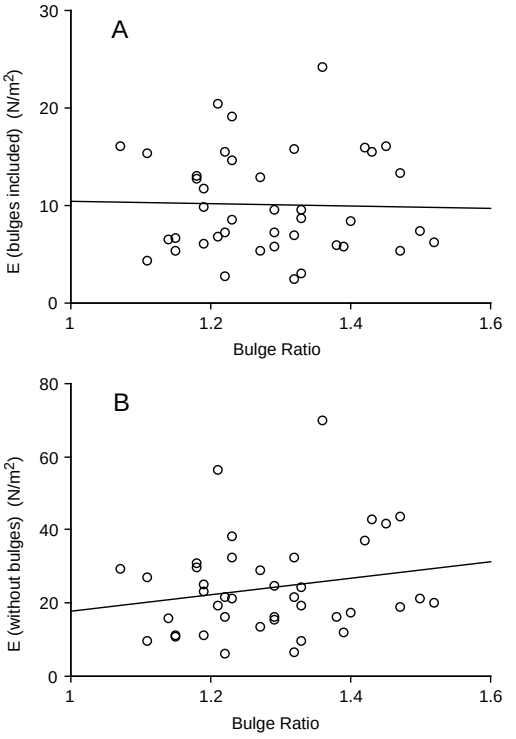

Fig. 6. Graphs of $E(50)$, calculated (A) with and (B) without including the contribution of bulges (see Fig. 5) to the explant's width and thickness when calculating stress and strain. The regression lines suggest that stiffnesses calculated by including bulges are less sensitive to the size of the bulges than stiffnesses calculated without the bulges.

Does IMZ stiffness change during development?

The mean $E(180)$ of the IMZ along its anteroposterior axis, which is the normal axis of extension, more than tripled between stage 10+ and stage 11.5 (Fig. 9; Table 1). This increase was highly significant (Mann-Whitney U: $P<0.0001$, n=34). In contrast, the stiffness along the mediolateral axis of the IMZ did not change significantly between stages 10+ and 11.5 (P=0.12, n=24). Thus, the increase in stiffening was anisotropic.

Is IMZ stiffness anisotropic?

At stage 10+, the mediolateral $E(180)$ was significantly greater

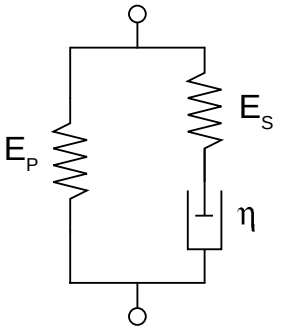

Fig. 7. Viscoelastic mechanical network model comprising a spring (elastic modulus=E_P) in parallel with a Maxwell element having a spring (elastic modulus=E_S) arranged in series with dashpot (viscosity=η).

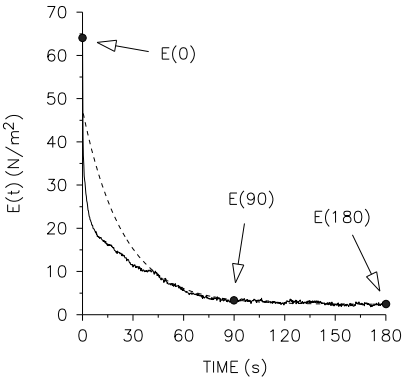

Fig. 8. Relaxation function (solid line) for a stage 11.5 IMZ explant under anteroposterior compression during a stress-relaxation test. The general shape of the curve resembles an exponential decay toward an asymptote and is typical of viscoelastic materials. The values of $E(t)$ at the three indicated times were used (see Appendix) to calculate a simple mathematical approximation to the data (dashed line), which was then used to obtain a network model describing the viscoelastic properties of the tissue.

than the anteroposterior $E(180)$ (P=0.02, n= 27), whereas, at stage 11.5, the anteroposterior and mediolateral $E(180)$s did not differ significantly (P=0.26, n=31) (Fig. 9; Table 1). Thus the IMZ is anisotropic at stage 10+, but not at stage 11.5.

Do IMZ cells deform or rearrange during stress relaxation?

The mesodermal cells of the IMZ (stage 10+ and stage 11.5 explants) were deformed but did not rearrange with respect to their neighbors during the stress-relaxation tests. The cells rapidly shortened along the axis of compression at the onset of the test but did not change their dimensions as the stress in the tissue decreased during the following 180 seconds (Fig. 10). None of the cells tracked (n=38) in stage 10+ and stage 11.5 explants moved relative to their neighbors during the 5-10 minutes of videorecording.

Does anteroposterior stiffening occur in other tissues?

Neither the prechordal mesoderm nor the vegetal endoderm increased significantly in anteroposterior stiffness between stages 10+ and 11.5 (prechordal mesoderm: P=0.12, n=14; vegetal endoderm: P=0.18, n=14) (Table 1).

Network models

The mechanical network model shown in Fig. 7 is the simplest model that captures the three most obvious features of the measured time-dependent modulus for each tissue sample: (1) a relatively high instantaneous stiffness followed by (2) a decay toward (3) a long-term stiffness. The stiffnesses (E_P and E_S) of the springs and the viscosity (η) of the dashpot in the network model describing the stress-relaxation behavior of IMZ, prechordal mesoderm and vegetal endoderm are presented in Table 2.

Table 1. Mean stiffness of different tissues at early and late gastrulation*

E(180) Units=N/m^2	IMZ (AP compr)	IMZ (ML compr)	Prechordal Mesoderm (AP compr)	Vegetal Endoderm (AP compr)
Early (Stage 10+)	**3.9** (1.5) n=15	**7.4** (4.0) n=12	**6.2** (1.2) n=7	**4.4** (2.1) n=7
Late (Stage 11.5)	**14.2** (7.6) n=19	**11.6** (6.8) n=12	**8.9** (5.2) n=7	**3.0** (1.6) n=7

*Table cells show: **mean** (s.d.) and n=number of samples; AP compr, anteroposterior compression; ML compr, mediolateral compression.

DISCUSSION

The dorsal IMZ increases in stiffness after involution and as convergent extension begins

Stress relaxation tests show that the dorsal IMZ increases in anteroposterior stiffness threefold from its preinvolution position at stage 10$^+$ (prior to onset of its convergent extension) to its postinvolution position at stage 11.5 (when convergent extension is well underway). This change in stiffness during convergent extension is significant for several reasons, which we discuss below.

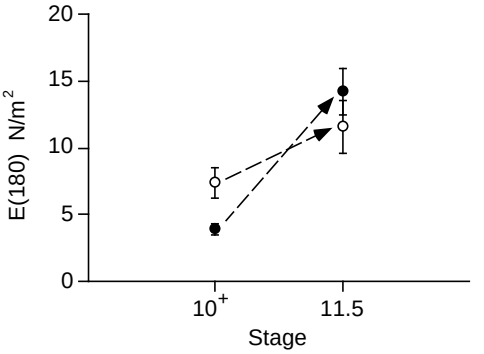

Fig. 9. Comparison of mean $E(180)$ of IMZ explants taken from early (stage 10$^+$) or late (stage 11.5) gastrulae compressed anteroposteriorly (filled circles) or mediolaterally (open circles). Error bars are s.e.m. At stage 10$^+$, the IMZ is significantly stiffer in mediolateral compression than in anteroposterior compression. Resistance to anteroposterior compression increases significantly between stage 10$^+$ and 11.5.

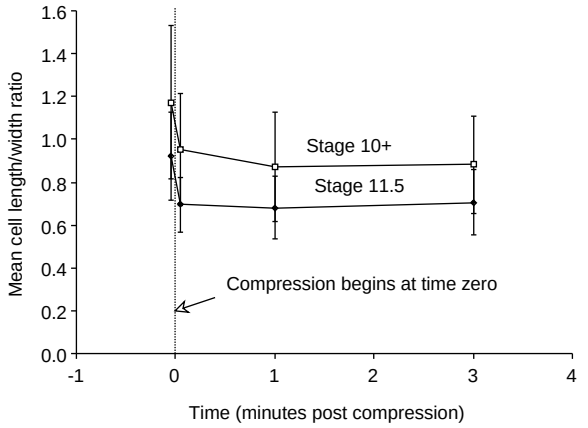

Fig. 10. Graph of cell mean length-to-width ratio as a function of time after strain application. The cell shapes change when compression is first applied, but remain relatively constant thereafter, suggesting that intracellular processes, rather than cell rearrangements, account for the decrease in stress observed during the stress-relaxation tests. Error bars are s.d.

Postinvolution stiffening is developmentally regulated

These measurements establish that the dorsal mesodermal-endodermal tissues are relatively deformable prior to involution, thus allowing them to bend around the blastopore lip, but become stiffer after involution, during convergent extension. This is not a general property of the embryo, since neither the prechordal mesoderm nor the vegetal endoderm show a corresponding increase in stiffness. This stiffening may follow the anteroposterior progression shown by other mesodermal processes, including mediolateral cell intercalation behavior, which begins anteriorly and progresses posteriorly such that the posterior boundary of the progression always lies right at the blastopore lip (Shih and Keller, 1992b; Keller et al., 1992). We can test this by using smaller explants to improve spatial resolution.

Postinvolution stiffening supports embryonic axis elongation

Adequate stiffness is essential for the IMZ to elongate the embryonic axis without buckling. Presumably IMZ extension forces of up to 0.6 μN (Moore, 1994), together with those generated by the parallel extension of the dorsal NIMZ, are sufficient to narrow and elongate the dorsal axis itself and to overcome the resistance of passively deformed surrounding tissues, of which there are three: (1) the vegetal endoderm of the yolk plug, which becomes reshaped and squeezed into the interior of the gastrula during blastoporal closure, (2) the dorsolateral mesoderm just lateral to the somitic mesoderm, which becomes stretched, and (3) the dorsolateral epidermis just lateral to the neural plate, which also becomes stretched. Measurement of the combined stiffness and force production of the dorsal IMZ and NIMZ together and the stiffness of the dorsolateral epidermis and mesoderm together would address this issue.

Increased anteroposterior stiffness is due to reinforcement of the cytoskeleton or extracellular matrix

The increased stiffness of the IMZ along the anteroposterior axis could, in principle, be due to increased cell-cell or cell-matrix adhesion, increased stiffness of the cytoskeleton, increased stiffness of the extracellular matrix, or some combination of these. Since cells in both early (stage 10+) and late (stage 11.5) IMZ explants are deformed, but are not rearranged, during three-minute stress-relaxation tests, adhesion strength must be large enough to prevent cell slippage. Therefore, both the viscoelastic relaxation and the ontogenetic changes in stiffness that we measured must reflect mechanical properties of the cytoskeleton, ECM, or both, rather than those of cell-cell or cell-matrix adhesion. This is not to say that adhesion is not important to the mechanics of the tissue (it is essential for tissue integrity and traction between cells), nor that adhesion does not change (it must be dynamic to allow mediolateral cell intercalation, which occurs over time intervals longer than our tests), but only that adhesion was not a source of the dynamic relaxation we measured during our tests.

We believe that tissue stiffening may be accompanied by reinforcement of the cytoskeleton, either by compression-resisting elements oriented parallel to the long axis of the embryo (the short axis of the cells) or by tension-resisting elements oriented along the mediolateral axis of the embryo (the long axis of the cells). Because the cells appear to pull themselves between one another as a result of mediolaterally directed protrusive activity (Shih and Keller, 1992a) (Fig. 2), they are probably under tension in the mediolateral direction and under compression in the anteroposterior direction. We propose that the cytoskeleton is reinforced by tension-resisting elements parallel to the mediolateral axis of the embryo as convergent extension begins. Microtubules of the dorsal mesodermal cells become aligned with the mediolateral axis of the embryo at early stages of convergent extension and, at late stages, they remain aligned mediolaterally and also become restricted to the cortex of the cells (Lane and Keller, 1994). We are currently testing the potential role of these microtubules in

Table 2. Network model values*

		IMZ (AP compr)	IMZ (ML compr)	PreCh Meso (AP compr)	Veg Endo (AP compr)
Stage 10+	E_P (N/m^2)	3.6 (1.6)	7.1 (4.1)	5.6 (1.2)	4.2 (1.7)
	E_S (N/m^2)	17.7 (5.4)	20.5 (7.7)	9.0 (4.2)	19.2 (5.3)
	η (N•s/m^2)	630 (330)	760 (480)	210 (180)	500 (150)
Stage 11.5	E_P (N/m^2)	13.7 (7.4)	11.1 (6.9)	8.5 (5.1)	2.9 (1.4)
	E_S (N/m^2)	30.1 (16.2	29.0 (12.3)	12.7 (8.1)	20.6 (5.1)
	η (N•s/m^2)	960 (750)	1110 (610)	420 (380)	580 (270)

*Table cells show: mean (s.d.); AP compr, anteroposterior compression; ML compr, mediolateral compression.

stiffening these explants. We do not yet have appropriate structural information on the arrangement of actin microfilaments and intermediate filaments in these cells.

Extracellular matrix (ECM) is found between the cells of the dorsal involuted mesoderm (reviewed in Johnson et al., 1992), and several cell matrix receptors are expressed in this region (DeSimone, 1994; Ransom et al., 1993). Recently, a *Xenopus* homologue of the fibrillin family of extracellular matrix molecules has been found to be expressed in the dorsal, axial mesoderm and may function in convergent extension (P. M. Skoglund, personal communication). The ECM could contribute to the overall increase in explant stiffness by functioning as a continuous extracellular mechanical element, independent of the cells, or it could act as a ligand between cells, transmitting forces from one cell to the next. Even if ECM is the primary stress-bearing element, cell-matrix or cell-cell adhesions (or both) must be present to explain the observed lack of cell rearrangements during the stress-relaxation tests.

Biomechanical analysis of cell-cell and cell-matrix adhesions

Our findings suggest a biomechanical approach to analysis of cell-cell and cell-matrix adhesion in gastrulation. If the function of cell-cell adhesion is reduced progressively by a dominant negative disruption of cadherin function (Kintner, 1992) until adhesion, rather than cytoskeletal or ECM stiffness, becomes the 'weak link' in the chain of force transmission, then convergent extension will be less effective and gastrulation should fail at the midgastrula stage (stage 10.5-11), when convergent extension becomes important (Keller et al., 1992). In these embryos, we expect cadherin disruption to cause a decrease in tissue stiffness and an increase in cell rearrangements during stress-relaxation tests. Conversely, we expect that overexpression of adhesion molecules (e.g., Detrick et al., 1990; Fujimori et al., 1990) would not improve convergent extension under its normal load, since the normal adhesions appear to be adequate. In fact, overexpression of adhesion molecules may retard convergent extension, either directly, by interfering with dynamic exchange of adhesions during cell intercalation, or indirectly, by making adjacent tissues too stiff to stretch, depending on where overexpression occurred.

Network model data for mathematical models of morphogenesis

The network models (Fig. 7 combined with the element values in Table 2) given here provide a quantitative description of the stress-relaxation properties of each tissue in a format that can be incorporated directly into mathematical models of morphogenetic processes involving those tissues. The significance of these network model data best awaits interpretation through mathematical models based on that data – the network models presented in this paper are *descriptions* of measured mechanical properties, *not explanations* for them. Correlations between elements in the network models and specific components or processes within the embryo are neither implied nor denied.

In conclusion

Morphogenesis is fundamentally a mechanical process. Therefore, an understanding of force production and mechanical properties within embryonic tissues is essential to a complete understanding of how genes and gene products, including the cytoskeleton, ECM and cell adhesions, function in morphogenesis. We have used standard engineering approaches (stress-relaxation tests and mechanical network models) to quantify the time-dependent elastic modulus (stiffness) of IMZ, prechordal mesodermal and vegetal endodermal tissues from *X. laevis* gastrulae. Our results illuminate the mechanical basis of convergent extension and gastrulation, and they provide both baseline data and direction for mathematical models and experiments testing how events at the molecular level generate the forces and regulate the tissue mechanical properties that drive morphogenesis in embryos.

This research was supported by NSF Grant no. FD92-20525 to R. Keller and M. Koehl, and by a MacArthur Foundation Fellowship Award to M. Koehl. The Histowiggler was developed with the support of NIH grant no. NIDCD-00112 to E. R. Lewis. We are grateful to J. Goldman for technical assistance and to S. Worcester for help with the statistical analyses.

APPENDIX

The three-element network models used to describe quantitatively the elastic and viscous properties of the tissues discussed in this paper were obtained by first approximating the measured stress-relaxation functions with a simple equation and then identifying a network model with viscoelastic behavior described by the same equation.

Curve-fitting

Relaxation functions in biological materials are complicated and result from mechanical processes interacting across many different organizational levels and time scales (Fung, 1977). The goal of our network modeling efforts was to obtain the simplest possible model that still quantified the essential features of stiffness and viscoelastic relaxation in the tissues we measured.

We approximated each measured relaxation function, $E_m(t)$, with a simplified relaxation function, $E(t)$, corresponding to an exponential decay toward a final asymptotic modulus value (E_∞):

$$E(t) = E_\infty + Ce^{-t/\tau}, \quad [1]$$

where C is an additional stiffness seen in response to quickly applied strains, and τ is a time constant describing how quickly the additional stiffness 'fades away' during relaxation of the tissue.

Any three points on the curve described by the equation are sufficient to determine uniquely the values of the three parameters in the equation. A simple method we used for fitting the equation to each of our empirical stress-relaxation functions was to require that the descriptive curve match the empirical curve at three evenly spaced times:

$$\begin{aligned} E_m(t_1) &= E_\infty + Ce^{-t_1/\tau}, \\ E_m(t_2) &= E_\infty + Ce^{-t_2/\tau}, \\ E_m(t_3) &= E_\infty + Ce^{-t_3/\tau}. \end{aligned} \quad [2]$$

To capture both the instantaneous stiffness and the long-term

stiffness, we chose t_1=0, t_2=90, and t_3=180 seconds (see Fig. 8). (To reduce noise, we averaged three samples near each time, specifically those at t, t+0.25, and t+0.50 seconds). Rearranging, and taking quotients:

$$\frac{E_m(t_1)-E_\infty}{E_m(t_2)-E_\infty}=\frac{Ce^{-t_1/\tau}}{Ce^{-t_2/\tau}}=e^{(t_2-t_1)/\tau}$$
$$\frac{E_m(t_2)-E_\infty}{E_m(t_3)-E_\infty}=\frac{Ce^{-t_2/\tau}}{Ce^{-t_3/\tau}}=e^{(t_3-t_2)/\tau}. \quad [3]$$

Since we chose our three time intervals with equal spacing,

$$(t_2-t_1)=(t_3-t_2).$$

Therefore,

$$\frac{E_m(t_1)-E_\infty}{E_m(t_2)-E_\infty}=\frac{E_m(t_2)-E_\infty}{E_m(t_3)-E_\infty}.$$

Solving for E_∞ yielded

$$E_\infty=\frac{E_m(t_1)E_m(t_3)-E_m(t_2)^2}{E_m(t_1)+E_m(t_3)-2E_m(t_2)}.$$

Then we took the natural logarithm of one of the equations in [3] and rearranged to solve for τ:

$$\ln\left[\frac{E_m(t_1)-E_\infty}{E_m(t_2)-E_\infty}\right]=\ln[e^{(t_2-t_1)/\tau}]=\frac{(t_2-t_1)}{\tau}.$$
$$\therefore\tau=\frac{(t_2-t_1)}{\ln\left[\frac{E_m(t_1)-E_\infty}{E_m(t_2)-E_\infty}\right]}.$$

Finally, we solved for C by rearranging one of the equations in [2]:

$$C=\frac{E_m(t_1)-E_\infty}{e^{-t_1/\tau}}.$$

The quality of the fit was evaluated by visually comparing the measured data with the descriptive curve defined by these parameters (see Fig. 8). In all cases, the description obtained by this procedure matched well both the initial height and the long-term behavior of the empirical curve, though stiffness values for intermediate times were consistently overestimated. We tested an equation involving two decaying exponential terms, which improved the fit, but its time constants invariably bracketed the time constant in the simple equation, suggesting the single time constant provides a good intermediate value for viscosity, so we used the simpler equation.

Network model

The mechanical network model in Fig. 7 has a relaxation function of the form described by equation [1] (see Findley et al., 1976). The overall stress in the model is the sum of the stresses in the left and right sides taken separately.

The left side is just a spring, so its stress relaxation function is a constant value given by the modulus of the spring:

$$E_{left}(t)=E_P.$$

The right side is only slightly more complicated. This series arrangement of a spring and dashpot is known as a Maxwell model, and it has a relaxation function given by:

$$E_{right}(t)=E_S e^{-t(\eta/E_S)}.$$

Thus the overall relaxation function for the model is given by

$$E(t)=E_{left}(t)+E_{right}(t)=E_P+E_S e^{-t/(\eta/E_S)}.$$

The network behavior can be made identical to [1] by setting:

$$E_P=E_\infty,\quad E_S=C,\quad \text{and}\quad \eta=E_S\tau.$$

REFERENCES

Akkas, N. (1987). *Biomechanics of Cell Division*. 374 p. New York: Plenum Press.

Akkas, N. ed. (1990). *Biomechanics of Active Movement and Deformation of Cells*. Berlin: Springer-Verlag.

Bereiter-Hahn, J., Anderson, O.R. and Reif, W.-E., eds., (1987) *Cytomechanics: The Mechanical Basis of Cell Form and Structure*. New York: Springer-Verlag.

Bray, D. (1992). *Cell Movements*. New York: Garland Publishing, Inc..

Condic, M. L., Fristrom, D. and Fristrom J. W. (1991). Apical cell shape changes during *Drosophila* imaginal leg disc elongation: A novel morphogenetic mechanism. *Development* **111,** 23-34.

Davidson, L. A., Koehl, M. A. R., Keller, R. E., and Oster, G. F. (1995). How do sea urchins invaginate? Using biomechanics to distinguish between mechanisms of primary invagination. *Development* **121**, 2005-2018.

DeSimone, D. W. (1994). Integrin function in early vertebrate development: perspectives from studies of amphibian embryos. In *Integrins: The Biological Problems.* (ed. Y. Takada). pp. 217-234. Boca Raton, Fla.: CRC Press.

Detrick, R., Dickey, D. and Kintner, C. (1990). The effects of N-cadherin misexpression on morphogenesis in *Xenopus* embryos. *Neuron* **4**, 493-506.

Ettensohn, C. A. (1985). Gastrulation in the sea urchin embryo is accompanied by the rearrangement of invaginating epithelial cells. *Dev. Biol.* **112**, 383-390.

Ferry, J. D. (1970). *Viscoelastic Properties of Polymers*, 2nd edition, John Wiley & Sons, Inc.

Findley, W. N.,Lai, J. S. and Onaran, K. (1976). *Creep and Relaxaationn of Nonlinear Viscoelastic Materials, with and Introduction to Linear Viscoelasticity*. New York: Dover Publications.

Finer, J., R. Simmons and J. Spudich (1994). Single myosin molecule mechanics: piconewton forces and nanometre steps. *Nature* **368**, 113-119.

Fujimori, T., Miyatani, S. and Takeichi, M. (1990). Ectopic expression of N-cadherin perturbs histogenesis in *Xenopus* embryos. *Development* **110**, 97-104.

Fung, Y.C. (1977). *Biomechanics: Mechanical Properties of Living Tissues.* New York, Heidleberg: Springer-Verlag.

Hardin, J. and Cheng, L. Y. (1986). The mechanisms and mechanics of archenteron elongation during sea urchin gastrulation. *Dev. Biol.* **115**, 490-501.

Irvine, K. D. and Wieschaus, E. (1994). Cell intercalation during *Drosophila* germband extension and its regulation by pair-rule segmentation genes. *Development* **120**, 827-841.

Ishijima, A., T. Doi, K. Sakurada and T. Yanagida (1991). Sub-piconewtonforce fluctuations of actomyosin in vitro. *Nature* **352**, 301-306.

Jacobson, A. G. (1981). Morphogenesis of the neural plate and tube. In *Morphogenesis and Pattern Formation*. (ed. T. G. Connelly, L. L. Brinkley and B. M. Carlson). pp. 233-282. New York: Raven Press.

Johnson, K. E., Boucaut, J. C. and DeSimone, D. (1992). The role of the

extracellular matrix in amphibian gastrulation. *Current Topics in Dev. Biol.* **27**, 91-127.

Kay, B. and Peng, B., eds. (1991). *Methods in Cell Biology, Vol. 36,* Xenopus laevis*: Practical Uses in Cell and Molecular Biology*. San Diego: Academic Press.

Keller, R. E. (1975). Vital dye mapping of the gastrula and neurula of *Xenopus laevis*. I. Prospective areas and morphogenetic movements of the superficial layer. *Dev. Biol.* **42**, 222-241

Keller, R.E. (1976). Vital dye mapping of the gastrula and neurula of *Xenopus laevis*. II. Prospective areas and morphogenetic movements in the deep region. *Dev. Biol.* **51**, 118-137.

Keller, R. E. (1986). The cellular basis of amphibian gastrulation. In *Developmental Biology: A Comprehensive Synthesis. Vol. 2. The Cellular Basis of Morphogenesis.* (ed. L. Browder). pp. 241-327. New York: Plenum Press.

Keller, R. E. (1991). Early embryonic development of Xenopus laevis. In *Methods in Cell Research, Vol. 36, Xenopus laevis: Practical Uses in Cell and Molecular Biology*. (ed. B. Kay and B. Peng). pp. 61-113. San Diego: Academic Press.

Keller, R. E. and Danilchik, M. (1988). Regional expression, pattern, and timing of convergence and extension during gastrulation of *Xenopus laevis*. *Development* **103**, 193-209.

Keller, R. E. and Jansa, S. (1992). *Xenopus* gastrulation without a blastocoel roof. *Developmental Dynamics* **195**, 162-176

Keller, R. E., Shih, J. and Domingo, C. (1992). The patterning and functioning of protrusive activity during convergence and extension of the *Xenopus* organiser. *Development* **1992 Supplement**, 81-91.

Keller, R. E., Shih, J. and Wilson, P. (1991). Cell motility, control and function of convergence and extension during gastrulation in *Xenopus*. In *Gastrulation: Movements, Pattern, and Molecules*. (ed. R. Keller, W. Clark and F. Griffen). pp. 101-119. New York: Plenum Press.

Keller, R. E. and Winklbauer, R. (1992). Cellular basis of amphibian gastrulation. *Current Topics in Developmental Biology* **27**, 39-89

Kintner, C. (1992). Regulation of embryonic cell adhesion by the cadherin cytoplasmic domain. *Cell* **69**, 225-236.

Koehl, M. A. R. (1990) Biomechanical approaches to morphogenesis. *Semin. Devel. Biol.* **1**, 367-378.

Koehl, M., Adams, D. and Keller, R. (1990). Mechanical development of the notochord in early tailbud embryos. In: *Biomechanics of Active Movement and Deformation of Cells.* pp. 471-485. Berlin, NY: Springer-Verlag.

Lane, M. C. and Keller, R. E. (1994). Radical reorganization of microtubules in the axial mesoderm during *Xenopus* morphogenesis. *Mol. Biol. Cell* **5 (Suppl)**, 101a (abs. #584).

Mittenthal, J. E. and Jacobson, A. G. (1990). The mechanics of morphogenesis in multicellular embryos. In *Biomechanics of Active Movement and Deformation of Cells*. (ed. N. Akkas). pp. 295-401. Berlin: Springer-Verlag.

Miyamoto, D. M. and Crowther, R. (1985). Formation of the notochord in living ascidian embryos. *J. Embryol. Exp. Morphol.* **86**, 1-17.

Moore, S.W. (1992). Direct measurement of dynamic biomechanical properties of amphibian embryonic tissues. Ph.D. dissertation, University of California, Berkeley.

Moore, S.W. (1994). A fiber optic system for measuring dynamic mechanical properties of embryonic tissues. *IEEE Transactions on Biomedical Engineering* **41**, 45-50.

Nieuwkoop, P. D. and Faber, J. (1967). *Normal Table of Xenopus laevis (Daudin).* Amsterdam: North-Holland.

Odell, G, Oster, G, Alberch, P. and Burnside, B. (1981). The mechanical basis of morphogenesis I. Epithelial folding and invagination. *Dev. Biol.* **85**, 446-462

Ransom, D. G., Hens, M. D. and DeSimone, D. W. (1993). Integrin expression in early amphibian embryos: cDNA cloning and characterization of Xenopus b1, b2, b3, and b6 subunits. *Dev. Biol* **160**, 265-275.

Sater, A. K., Steinhardt, R. A. and Keller, R. (1993) Induction of neuronal differentiation by planar signals in *Xenopus* embryos. *Develop. Dynamics* **197**, 268-280.

Scharf, S. R. and Gerhart, J. C. (1980). Determination of the dorsal-ventral axis in eggs of *Xenopus laevis*: complete rescue of uv-impaired eggs by oblique orientation by first cleavage. *Dev. Biol.* **79**, 181-198.

Schoenwolf, G. C. and Alvarez, I. S. (1989). Roles of neuroepithelial cell rearrangement and division in shaping of the avian neural plate. *Development* **106**, 427-439.

Schoenwolf, G. C. and Smith, J. (1990). Mechanisms of neurulation: Traditional viewpoint and recent advances. *Development* **109**, 243-270.

Shih, J. and Keller, R. E. (1992a). Cell motility driving mediolateral intercalation in explants of *Xenopus laevis*. *Development* **116**, 901-914

Shih, J. and Keller, R. E. (1992b). Patterns of cell motility in the organizer and dorsal mesoderm of *Xenopus laevis*. *Development* **116**, 915-930

Spemann, H. (1938) *Embryonic Development and Induction.* Newhaven, CT: Yale U. Press.

Svoboda, K. and S. Block (1994). Force and velocity measured for single kinesin molecules. *Cell* **77**, 773-84.

Trinkaus, J. P., Trinkaus, M. and Fink, R. D. (1992). On the convergent cell movements of gastrulation in *Fundulus*. *J. Exp. Zool.* **261**, 40-61.

Vincent, J. (1990) *Structural Biomaterials*, revised edition. Princeton, NJ: Princeton Univ. Press.

Vogel, S. (1988). *Life's Devices: The Physical World of Animals and Plants*. Princeton, NJ: Princeton Univ. Press,

Vogel, S. (1994). *Life in Moving Fluids: The Physical Biology of Flow*. (2nd ed.) Princeton, NJ: Princeton University Press.

Vogt, W. (1929). Gestaltungsanalyse am Amphibienkeim mit ortlicher Vitalfarbung. II. Teil. Gastrulation und Mesodermbildung bei Urodelen und Anuren. *Wilhelm Roux Arch. EntwMech. Org.* **120**, 384-706.

Wainwright, S. A., Biggs, W. D., Currey, J. D. and Gosline, J. M. (1976). *Mechanical Design in Organisms*. London: Edward Arnold.

Warga, R. M. and Kimmel, C. B. (1990). Cell movements during epiboly and gastrulation in zebrafish. *Development* **108**, 569-580.

Weliky, M, Minsuk, S., Keller, R. and Oster, G. (1991). The mechanical basis of cell rearrangement II. Notochord morphogenesis in *Xenopus laevis*: Simulation of cell behavior underlying tissue convergence and extension. *Development* **113**, 1231-1244.

Weliky, M. and Oster, G. (1990). The mechanical basis of cell rearrangement: I. Epithelial morphogenesis during *Fundulus* epiboly. *Development* **109**, 373-386.

Winklbauer, R., Selchow, A., Nagel, M., Stoltz, C. and Angres, B. (1991). Mesoderm cell migration in the *Xenopus* gastrula. In *Gastrulation: Movements, Patterns and Molecules*. (ed. R. Keller, W. Clark and F. Griffin). pp. 147-168. New York: Plenum Press

(Accepted 7 July 1995)